International Journal of Optics and Applications 2015, 5(4): 121-132
DOI: 10.5923/j.optics.20150504.03

Modeling and Analysis of a Miniaturized Ring Modulator Using Silicon-Polymer-Metal Hybrid Plasmonic Phase Shifter. Part I: Theoretical Framework

Alhuda A. Al-mfrji[1], Shelan K. Tawfeeq[1], Raad S. Fyath[2,*]

[1]Institute of Laser for Postgraduate Studies, University of Baghdad, Iraq
[2]College of Engineering, Al-Nahrain University, Iraq

Abstract This paper presents comprehensive analysis and investigation for 1550nm and 1310nm ring optical modulators employing an electro-optic polymer infiltrated silicon-plasmonic hybrid phase shifter. The paper falls into two parts which introduce a theoretical modeling framework and performance assessment of these advanced modulators, respectively. In this part, analytical expressions are derived to characterize the coupling effect in the hybrid phase shifter, transmission function of the modulator, and modulator performance parameters. The results can be used as a guideline to design compact and wideband optical modulators using plasmonic technology.

Keywords Ring modulator, Hybrid plasmonic phase shifter, Electro-optic polymer

1. Introduction

Silicon-based photonic integrated circuits (PICs) are an attractive solution for next generation high-speed data transmission [1, 2]. Usually these circuits are realized using standard complementary metal-oxide semiconductor (CMOS) fabrication technology [3, 4] where silicon photonics offer low cost, low power consumption, and high bandwidth [2]. Recently silicon PICs have been demonstrated for both intra- or inter chip -link, and long haul telecommunication links [2]. Optical interconnects have recently emerged as promising solution for alleviating the bandwidth in modern computing electronics [5]. As a key part of optical interconnect on silicon chips, electro-optic (EO) modulators have been made great progress in recent years and attracted many interests [6]. In addition to that, optical networks have been growing up and integrated components such as optical modulators are widely developed and employed as key components for such application. Especially, the next generation optical networks are demanded to have the features of high capacity, high-speed and high- agility which require the aggregate carrier data per optical fiber to be extended toward 100 Tb/s [7]. This requires high performance modulators capable to deal with ultrahigh speed data rate of single-channel optical signals (100 Gb/s and higher in the future compared with current 10 and 40 Gb/s) [7, 8].

Conventional CMOS-compatible silicon optical modulator are usually realized using the linear EO (Pockels) effect rather than carrier depletion effect in order to achieve high speed operation [9-11]. Unfortunately, these modulators suffer from two main limitations

(i) CMOS compatibility sets limit to the required operating voltages [6]. Silicon is characterized by relatively low linear EO coefficients and hence requires relatively high modulating voltages. This problem has been solved by incorporating polymer with higher EO coefficient in the active region of the modulator leading to silicon-polymer hybrid modulators [12-15].

(ii) Advances in CMOS technology enable the fabrication of integrated electronics on nano-scale size. In contrast, the size of a conventional optical modulator is in order of operating wavelength or higher. A technology emerging recently which can scale down the dimensions of optical devices far beyond the diffraction limit is plasmonics [16]. This technology is based on surface plasmon polariton (SPP) which travels through a form of hybrid electrical/optical propagation [17-19]. A plasmon is a quasi-particle formed from the coupling of a photon and a travelling electron density wave at the interface between a metal and a dielectric [20]. Recently, plasmonic technology has been used to realize ultra-compact modulators suitable for integration with electronic components and hence meet footprint and efficiency requirement of PICs [21].

* Corresponding author:
rsfyath@nahrain-eng.org (Raad S. Fyath)
Published online at http://journal.sapub.org/optics

Several ultra-compact plasmonic modulators have been proposed in the literature for 50 Gb/s (and above) operation using silicon-metal [6, 22, 23] or silicon-polymer-metal hybrid structures [11, 24, 25]. The proposed modulators have been designed using Mach-Zehnder interference (MZI) [10, 22, 25-30], nonresonant (forward) waveguide [9, 15, 31-34], or microring resonator (MRR)-based structure [35-37]. Plasmonic modulator for high-level modulation have been also proposed using a combination of MZI and waveguide topologies [11-13]. The microring resonator attracts increasing interest as a promising photonic device for integrated optical interconnects and novel photonic architectures which can be implemented easily in silicon photonic platforms. The main advantages of this device are

(i) It can be configured either as an optical modulator or a wavelength division multiplexing drop filter [38].
(ii) It offers smaller footprint than the Mach-Zehnder modulator (MZM) [16].
(iii) When fabricated using silicon-on-insulator (SOI) platforms, the microning resonator exhibits a great potential to build space, power, and spectrally efficient on-chipphotonic networks that could be seamlessly integrated with CMOS electronics [39].
(iv) The microning modulator exhibits smaller chip size and capacitance, resonant-enhanced efficiency, and high wavelength selectively in comparison to MZM [39].
(v) When compared to MZM, ring resonator has the potential for low power consumption and array integration [40].

Unfortunately, the performance of MRRs is very sensitive to the operating wavelength, due to their high thermal sensitivity, and to the geometric and material parameter variations, due to their small size. Therefore, the design of microning modulators should be addressed carefully.

Recently, Xu et al. [36, 37] have proposed a race track ring-based optical modulator employing an EO polymer infiltrated silicon- plasmonic hybrid phase shifter. Their simulation results reveal a 15dB extinction ratio under 1.2V.

This paper presents comprehensive analysis and detailed performance investigation for this modulator structure when it is designed to operate at optical telecommunication wavelengths. The results can be used as a guideline to design ultra-compact and high speed plasmonic modulator suitable for implementation in CMOS platform. The first part of this paper constructs the theoretical framework required to design the modulator and develops general expressions to assess its performance. Simulation results related to modulator performance and its capability to be implemented in high bit rate optical communication systems are given in part II.

The simulation results stand heavily on COMSOL 4.3b and partially on OptiSystem 12 software packages.

2. Device Description and Design Methodology

The silicon-plasmonic racetrack modulator proposed in [36, 37] will be investigated in this paper. This modulator consists of racetrack resonator coupled to a bus waveguide as shown in Fig. 1. The plasmonic slot waveguide with EO organic cladding material is positioned above one of the straight arms (silicon waveguide) of the resonator. This principle is similar to directional coupling between two waveguides. The plasmonic photonic hybrid directional coupler consists of two arms. The upper arm is silver-polymer-silver plasmonic slot waveguide while the lower arm is silicon dielectric waveguide embedded in silicon di-oxide. Different widths of silicon waveguide are obtained according to phase matching condition corresponding to different polymer slot widths.

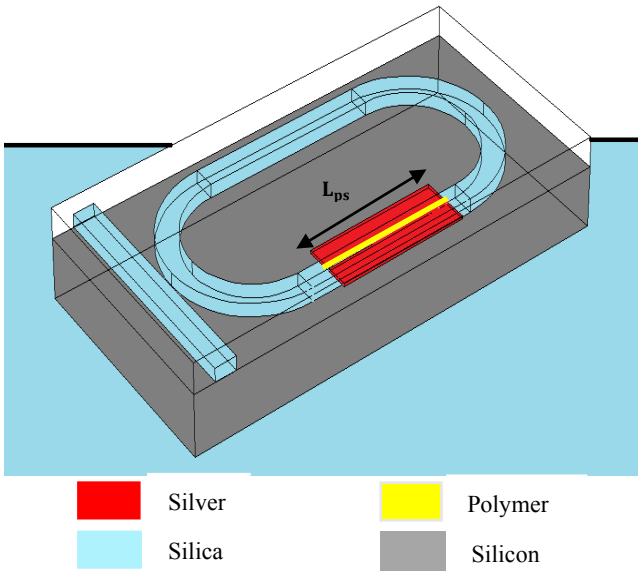

Figure 1. Structure of Silicon-plasmonic racetrackresonator modulator

Two guided eigen modes (quasi-even and quasi-odd modes) are formed consequently in the overlapping area between the two the photonic and plasmonic waveguides. The propagation constants of eigen modes being different, the power exchange between the waveguides can be represented as a beating between these two modes. The basic principle of the hybrid coupler is illustrated in Fig. 2.

The hybrid directional coupler can act as a phase shifter by applying static electric field (V_a/W_{sl}) via Pockels effect, where V_a is the modulating voltage and W_{sl} is polymer slot width. The refractive index of the polymer is changed by $\Delta n = 0.5\,\Gamma\gamma_{33}n_{poly}\,(V_a/W_{sl})$, where γ_{33} is EO coefficient, n_{poly} is the polymer refractive index, and Γ is the optical confinement factor of the slot. By modulating the refractive index of the polymer in the slot, the information is encoded in the phase of the SPP.

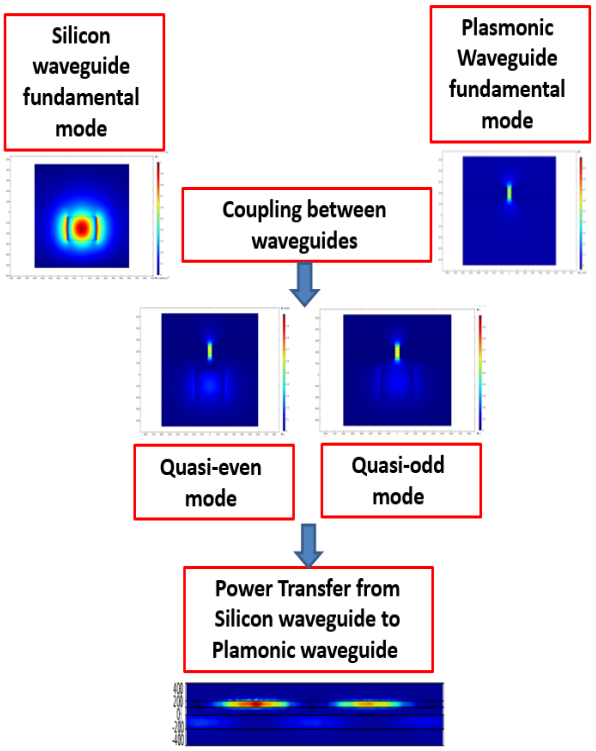

Figure 2. Basic principle of plasmonic photonic hybrid coupler

To design the hybrid phase shifter, some important factors should be taken into account.

(i) Phase matching condition: The real part of the effective refractive index of the fundamental photonic mode should be equal the real part of the effective refractive index of the fundamental plasmonic mode. This condition is satisfied for a specific polymer slot width as represented by the operating point A in Fig. 3. Thus the required silicon waveguide width W_{si} is obtained. Note that the effective index of the plasmonic mode is independent of W_{si}.

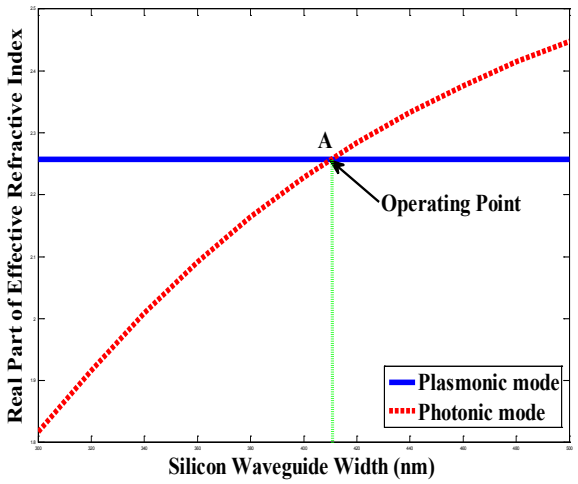

Figure 3. Real parts of the effective refractive indices of photonic and plasmonic modes as a function of silicon waveguide width

(ii) The length of the phase shifter should be equal even number of coupling length to ensure maximum transfer of power from the plasmonic waveguide to the optical waveguide at the end of the phase shifter. Coupling length is a measure of beating length of quasi-even and quasi-odd modes inside the coupler and can be related to propagation constants of the two eigen modes by $L_c = \pi/(\beta_e - \beta_o)$. Here β_e and β_o represent propagation constants for the quasi-even and quasi-odd modes, respectively.

3. Coupling between Silicon and Plasmonic Waveguides

The coupling between the modes of plasmonic waveguide and silicon waveguide can be investigated using the concept of parallel two-waveguide coupler as shown in Fig. 4. Both waveguides are assumed to be homogeneous along the direction of propagation (i.e., z axis) with refractive index distribution which is in general a function of x and y axes.

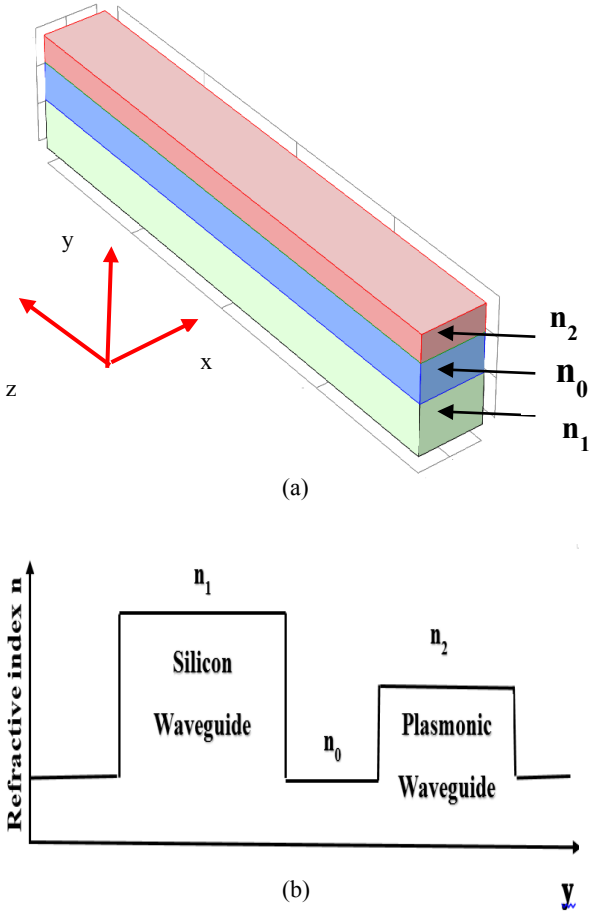

Figure 4. (a) Parallel two-waveguide coupler model to characterize the interaction between plasmonic and silicon waveguides. (b) Refractive index distribution in the transverse plane of the coupler

The refractive index distribution in the three layers of Fig. 4a can be expressed as

$$n(x,y)=\begin{cases} n_1(x,y) & \text{silicon waveguide} \\ n_0(x,y) & \text{background} \\ n_2(x,y) & \text{plasmonic waveguide} \end{cases} \quad (1)$$

When the two parallel waveguides are far apart, the electric field modes of propagation of the individual waveguides can be expressed as

$$\mathbf{e_1}(x,y,z,t)=\mathbf{E_1}(x,y)\exp[j(\omega t-\beta_1 z] \quad (2a)$$

$$\mathbf{e_2}(x,y,z,t)=\mathbf{E_2}(x,y)\exp[j(\omega t-\beta_2 z] \quad (2b)$$

When the two waveguides are separated by a short distance, the coupling effect should be taken into account. In this case, the electric field of the wave propagating in the coupled-waveguide structure can be expressed as [41]

$$\mathbf{e}(x,y,z,t)=A_1(z)\,\mathbf{e}_1(x,y,z,t)+A_2(z)\mathbf{e}_2(x,y,z,t) \quad (3)$$

where the mode amplitudes $A_1(z)$ and $A_2(z)$ are introduced to take into account the coupling effects along the axial direction of the waveguide.

The electric field of the propagating wave in the coupler strucure should obey the scalar wave equation

$$\nabla^2\mathbf{E}+\frac{\omega^2}{c^2}n^2(x,y)\mathbf{E}=0 \quad (4)$$

where $\mathbf{E}$ is the electrical field complex amplitude, $\nabla^2=\partial^2/\partial x^2+\partial^2/\partial y^2+\partial^2/\partial z^2$ is the Laplacian operator, c is the speed of light in vacuum, and

$$n^2(x,y)=n_0^2+\Delta n_1^2(x,y)+\Delta n_2^2(x,y) \quad (5a)$$

with

$$\Delta n_1^2(x,y)=\begin{cases} n_1^2(x,y)-n_0^2 & \text{silicon waveguide} \\ 0 & \text{elesewhere} \end{cases} \quad (5b)$$

$$\Delta n_2^2(x,y)=\begin{cases} n_2^2(x,y)-n_0^2 & \text{plasmonic waveguide} \\ 0 & \text{elesewhere} \end{cases} \quad (5c)$$

Note that the two functions $\Delta n_1^2(x,y)$ and $\Delta n_2^2(x,y)$ obey the orthogonality since they refer to separate transverse regions

$$\iint \Delta n_i^2\,\Delta n_j^2\,dxdy=\delta_{ij} \quad (6)$$

where $\delta_{ij}=1$ when $i=j$ and 0 when $i\neq j$.

The transverse behavior of the field in a waveguide can be described by using the wave equation [42, 43]

$$\nabla_t^2\mathbf{E}=\left[\left(\frac{\omega}{c}\right)^2 n^2(x,y)-\beta^2\right]\mathbf{E}=0 \quad (7)$$

where $\nabla_t^2=\nabla^2-\partial^2/\partial z^2$ is the transversal Laplacian operator. Therefore, the individual coupler waveguides modes satisfy these equations

$$\left[\nabla_t^2+\frac{\omega^2}{c^2}[n_0^2(x,y)+\Delta n_1^2(x,y)]\right]\mathbf{E}_1(x,y)=\beta_1^2\mathbf{E}_1(x,y) \quad (8a)$$

$$\left[\nabla_t^2+\frac{\omega^2}{c^2}[n_0^2(x,y)+\Delta n_2^2(x,y)]\right]\mathbf{E}_2(x,y)=\beta_2^2\mathbf{E}_2(x,y) \quad (8b)$$

Subsituting eqn. (3) into eqn. (4) and using the assumption of slow variation of mode amplitude over z yeilds

$$-2j\beta_1\frac{dA_1}{dz}\mathbf{E}_1\exp[j(\omega t-\beta_1 z]$$

$$+\frac{\omega^2}{c^2}\Delta n_1^2(x,y)A_2\mathbf{E}_2\exp[j(\omega t-\beta_2 z)]$$

$$=2j\frac{dA_2}{dz}\mathbf{E}_2\exp[j(\omega t-\beta_2 z)]$$

$$-\frac{\omega^2}{c^2}\Delta n_2^2(x,y)A_1\mathbf{E}_1\exp[j(\omega t-\beta_1 z] \quad (9)$$

In writing eqn. (9), eqns. (8a) and (8b) are used under the assumption that the two coupler waveguides are not too close suchthat

$$\iint \mathbf{E}_i^*.\mathbf{E}_j\,dxdy \ll \iint \mathbf{E}_i^*.\mathbf{E}_i\,dxdy \quad i,j=1,2 \text{ and } i\neq j \quad (10)$$

Taking the scalar product of eqn. (9) with $\mathbf{E}_1^*(x,y)$ and $\mathbf{E}_2^*(x,y)$, respectively, and integrating over the entire xy plane yields two-coupled mode equations

$$\frac{dA_1}{dz}=-j\kappa_{11}A_1-j\kappa_{12}A_2\exp[j(\beta_1-\beta_2)z] \quad (11a)$$

$$\frac{dA_2}{dz}=-j\kappa_{21}A_1\exp[-j(\beta_1-\beta_2)z]-j\kappa_{22}A_2 \quad (11b)$$

where

$$\kappa_{ij}=\frac{\omega}{4}\varepsilon_0\iint \Delta n_i^2(x,y)\mathbf{E}_i^*.\mathbf{E}_j\,dxdy$$
$$\text{for } i,j=1 \text{ and } 2 \text{ with } i\neq j \quad (12a)$$

and

$$\kappa_{ii}=\frac{\omega}{4}\varepsilon_0\iint \Delta n_j^2(x,y)\mathbf{E}_i^*.\mathbf{E}_i\,dxdy$$

where $j=2$ when $i=1$ and $j=1$ when $i=2$ (12b)

In eqns. (12), ε_0 represents the permitivity of vacuum.

The coupling constants κ_{11} and κ_{22} represent only a small correction to the propagation constants β_1 and β_2, respectively. The terms with κ_{11} and κ_{22} in eqn. (11) result from the dielectric perturbations to one of the waveguide dueto the presence of the other waveguide. Under the assumption that the individual waveguides modes are locallized almost totally in its waveguide, then according to eqn. (12b) one can set $\kappa_{11}=\kappa_{22}=0$. These leaves eqns. (11a) and (11b) with two coupling constants κ_{12} and κ_{21} which form a complex conjugate $\kappa_{12}=\kappa_{21}^*$. Under this assumption, eqns. (11a) and (11b) can be rewritten as

$$\frac{dA_1}{dz}=-j\kappa A_2\exp[j(\beta_1-\beta_2)z] \quad (13a)$$

$$\frac{dA_2}{dz}=-j\kappa A_1\exp[j(\beta_1-\beta_2)z] \quad (13b)$$

where $\kappa_{11}=\kappa_{22}^*$ is assumed to be real without loss of generality and set equals to κ.

Let $\Delta\beta=(\beta_1-\beta_2)/2$, $A_1=A\exp(j\Delta\beta z)$ and $A_2=B\exp(j\Delta\beta z)$. Equation (13a) becomes

$$A(j\Delta\beta)\exp(j\Delta\beta z)+\exp(j\Delta\beta z)\frac{dA}{dz}$$
$$=-j\kappa B\exp(-j\Delta\beta z)\exp(2j\Delta\beta z)$$

Then

$$\frac{dA}{dz} = -j\Delta\beta\, A - j\kappa B \quad (14a)$$

In similar way, one can arrive to the following equation starting from eqn. (13b)

$$\frac{dB}{dz} = -j\kappa A + j\Delta\beta\, B \quad (14b)$$

A general solution of eqns. (14a) and (14b) takes the form

$$A(z) = a_1 \exp(jqz) + a_2 \exp(-jqz) \quad (15a)$$

$$B(z) = b_1 \exp(jqz) + b_2 \exp(-jqz) \quad (15b)$$

where q is a complex propagation constant.

Subsituting eqns. (15a) and (15b) into eqns. (14a) yeilds

$$a_1(jq)\exp(jqz) + a_2(-jq)\exp(-jqz) = -j\Delta\beta[a_1 \exp(jqz) + a_2 \exp(-jqz)] - j\kappa[b_1 \exp(jqz) + b_2 \exp(-jqz)]$$

Then

$$(q + \Delta\beta)a_1 = -\kappa b_1 \quad (16a)$$

$$(-q + \Delta\beta)a_2 = -\kappa b_2 \quad (16b)$$

Similarly, subsituting eqns. (15a) and (15b) into eqn. (14b) yeilds

$$(q - \Delta\beta)b_1 = -\kappa a_1 \quad (16c)$$

$$-(q + \Delta\beta)b_2 = -\kappa a_2 \quad (16d)$$

The relations in eqns. (16) are satisfied with nonzero values of a_1, a_2, b_1 and b_2 if the possible values of q obey the following dispersion relation (obtained by setting the determinant of the cofficient matrix to be zero)

$$q = \pm[(\Delta\beta)^2 - \kappa^2]^{1/2} \quad (17)$$

Let eqns. (16) be solved under the following boundary conditions

(i) $A_2(z) = 0$ at z=0 which yeilds $b_1 = -b_2$.

(ii) $A_1(z) = 1$ at z=0 which yeilds $a_2 = 1 - a_1$.

Dividing eqn. (16a) by (16b) yields

$$\frac{(q + \Delta\beta)a_1}{(-q + \Delta\beta)(1 - a_1)} = -1$$

This gives

$$a_1 = \frac{q - \Delta\beta}{2q} \quad (18a)$$

$$a_2 = \frac{q + \Delta\beta}{2q} \quad (18b)$$

$$b_1 = -b_2 = \frac{q^2 - (\Delta\beta)^2}{2\kappa q} = -\frac{\kappa}{2q} \quad (18c)$$

Using eqn. (15b) with $b_1 = -b_2 = -\kappa/2q$ and recall that $A_2 = B\exp(-j\Delta\beta z)$ give

$$A_2(z) = -j\frac{\kappa}{q}\exp(-j\Delta\beta z)\sin(qz) \quad (19a)$$

Using eqns. (18a) and (18b) into eqn. (15a) and recall that $A_1 = A\exp(j\Delta\beta z)$ yeilds

$$A_1(z) = \exp(j\Delta\beta z)\left[\cos qz - j\frac{\Delta\beta}{q}\sin qz\right] \quad (19b)$$

4. Design Concepts of the Plasmonic Ring Modulator

Based on Fig. 5, the linear input-output relationship of the bus-ring coupler can be described by the matrix relation

$$\begin{pmatrix} E_3 \\ E_4 \end{pmatrix} = \begin{pmatrix} \tau & \kappa_i \\ -\kappa_i^* & \tau^* \end{pmatrix}\begin{pmatrix} E_1 \\ E_2 \end{pmatrix} \quad (20)$$

where

τ = Straight-through coupling coefficient between bus and ring waveguide.

κ_i = Cross-coupling coefficient between bus waveguide and ring waveguide.

The superscript * denotes the conjugated complex.

The round trip in the ring is given by

$$E_2 = \alpha \exp\left(-j\beta_{ph}(L - L_{ps})\right)E_4 t_{ps} \quad (21)$$

where

α = Round trip loss coefficient of the ring

β_{ph} = Propagation constant of the photonic mode

L = Ring circumference

L_{ps} = Phase shifter length

t_{ps} = Transmission function of the hybrid phase shifter

From eqn. (21)

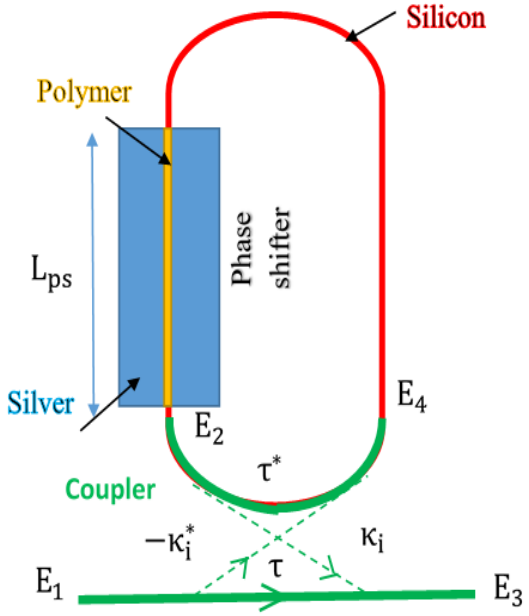

Figure 5. Model of single racetrack resonator with hybrid phase shifter and one bus waveguide

$$E_4 = \frac{E_2}{\alpha \exp\left(-j\beta_{ph}(L - L_{ps})t_{ps}\right)} \quad (22)$$

Substituting eqn. (20) into eqn. (22) yields

$$\frac{E_2}{E_1} = \frac{-\kappa_i^* \alpha \exp\left(-j\beta_{ph}(L - L_{ps})\right)t_{ps}}{1 - \alpha \exp\left(-j\beta_{ph}(L - L_{ps})\right)\tau^* t_{ps}} \quad (23a)$$

From eqn. (20)

$$E_3 = \tau E_1 + \kappa_i E_2 \quad (23b)$$

The transmission function of the ring modulator can be expressed as

$$\frac{E_3}{E_1} = \frac{\tau - \alpha \exp\left(-j\beta_{ph}\left(L - L_{ps}\right)\right)\left[|\tau|^2 + |\kappa_i|^2\right] t_{ps}}{1 - \alpha\tau^* \exp\left(-j\beta_{ph}\left(L - L_{ps}\right)\right) t_{ps}} \quad (24)$$

The transmission function of the hybrid phase shifter can be obtained from

$$t_{ps} = \frac{E_{ph}\left(L_{ps}\right)}{E_{ph}\left(0\right)} \quad (25)$$

where $E_{ph}\left(L_{ps}\right)$ is the electric field concentrated on silicon waveguide consisting the hybrid phase shifter. By using coupled mode theory between plasmonic waveguide and silicon waveguide and setting the plasmonic feild $E_{pl}(0) = 0$ yields

$$E_{ph}\left(L_{ps}\right) = A_1\left(L_{ps}\right)\exp\left(-L_{ps}/L_a\right)\exp\left(-j\beta_{ph}L_{ps}\right)E_{ph}\left(0\right) + A_2\left(L_{ps}\right)\exp\left(-L_{ps}/L_a\right)\exp\left(-j\beta_{ph}ps\right)E_{pl}\left(0\right) \quad (26)$$

where L_a is the mean attenuation length of the hybrid waveguide $= 2/\beta_{pli} = (2\pi/\lambda)n_{pli}$. Here n_{pli} is the imaginary part of the effective refractive index of the plasmonic mode n_{pl}.

The transmission function of the hybrid phase shifter can be written as

$$t_{ps} = e^{-L_{ps}/L_a} e^{-j(\beta_{ph} - \delta)}\, q\left(L_{ps}\right) \quad (27a)$$

where

$$q\left(L_{ps}\right) = \cos\left(sL_{ps}\right) - j(\delta/s)\sin\left(sL_{ps}\right) \quad (27b)$$

In eqn. (27a), δ is the phase velocity mismatch between the silicon waveguide photonic mode and the metal-dielectric-metal (MDM) plasmonic mode [37]

$$\delta = \left(\beta_{ph} - \beta_{plr}\right)/2 \quad (28a)$$

where $\beta_{ph} = 2\pi n_{ph}/\lambda$ is the propagation constant of the silicon waveguide mode whose effective index n_{ph} is assumed to be real (lossless waveguide). Further, β_{plr} is the real part of the complex propagation constant of the MDM plasmonic mode

$$\beta_{pl} = \beta_{plr} + j\beta_{pli} = \frac{2\pi}{\lambda}\left(n_{plr} + jn_{pli}\right) \quad (28b)$$

where $n_{plr} + jn_{pli}$ is the complex effective index of the plasmonic mode.

In eqn. (27b), the parameter s is defined as [37]

$$s = \sqrt{|\kappa_i|^2 + |\delta|^2} \quad (28c)$$

The coupling length $L_c = \pi/2s$.

By assuming that coupler's transmission and coupling coefficients are related by $[|\tau|^2 + |\kappa_i|^2] = 1$ (i.e., lossless coupler), then eqn. (24) becomes

$$t_{out} \equiv \frac{E_3}{E_1} = \frac{\tau - \alpha_{eff}\, t_{ps} \exp\left(-j\beta_{ph}\left(L - L_{ps}\right)\right)}{1 - \alpha_{eff}\, \tau\, t_{ps} \exp\left(-j\beta_{ph}\left(L - L_{ps}\right)\right)} \quad (29)$$

Substituting eqns. (27a) and (27b) into eqn. (29) yields where $\alpha_{eff} = \alpha\, e^{-L_{ps}/L_a}$ which reflects the effective loss of the resonator.

$$t_{out} = \frac{\tau - \alpha_{eff} \exp\left(-j\beta_{ph}\left(L - L_{ps}\right)\right) q\left(L_{ps}\right)}{1 - \alpha_{eff}\, t \exp\left(-j\beta_{ph}\left(L - L_{ps}\right)\right) q\left(L_{ps}\right)} \quad (30)$$

Equation (30) can be rewritten as

$$t_{out} = \frac{g\,\tau - \alpha_{eff}}{g - \alpha_{eff}\,\tau} \quad (31)$$

where

$$g \equiv g_m e^{jg} = e^{j(\beta_{ph}\, L - \delta\, L_{ps})}/q \quad (32a)$$

$$g_m = \left[\cos^2\left(s\, L_{ps}\right) + (\delta/s)^2 \sin^2\left(s\, L_{ps}\right)\right]^{-1/2} \quad (32b)$$

$$\theta_g = \beta_{ph} L - \delta\, L_{ps} + \tan^{-1}\left[\frac{(\delta/s)\sin\left(s\, L_{ps}\right)}{\cos(s\, L_{ps})}\right] = \beta_{ph} L - \delta\, L_{ps} + \tan^{-1}\left[(\delta/s)\tan\left(s\, L_{ps}\right)\right] \quad (32c)$$

Equation (31) can be rewritten as

$$t_{out} = \frac{g_m\, \tau\, e^{j\theta_g} - \alpha_{eff}}{g_m e^{j\theta_g} - \alpha_{eff}\, \tau}$$

The power transfer function is given by

$$T_{out} = |t_{out}|^2 = \frac{\left(g_m\, \tau \cos\theta_g - \alpha_{eff}\right)^2 + \left(g_m\, \tau \sin\theta_g\right)^2}{\left(g_m\, \tau \cos\theta_g - \alpha_{eff}\, \tau\right)^2 + \left(g_m \sin\theta_g\right)^2} = \frac{\alpha_{eff}^2 + g_m^2\tau^2 - 2g_m\alpha_{eff}\,\tau\cos\theta_g}{g_m^2 + \alpha_{eff}^2\tau^2 - 2g_m\alpha_{eff}\,\tau\cos\theta_g} \quad (33)$$

The minimum and maximum values of T_{out}, T_{min} and T_{max}, can be obtained by searching for the values of θ_g which leads to $dT_{out}/d\theta_g = 0$. The following equation is obtained under this condition (see eqn. (33)).

$$\left(g_m^2 + \alpha_{eff}^2\,\tau^2 - 2g_m\alpha_{eff}\,\tau\cos\theta_g\right)\sin\theta_g = \left(g_m^2 + \alpha_{eff}^2 - 2g_m\alpha_{eff}\,\tau\cos\theta_g\right)\sin\theta_g$$

Values of θ_g that satisfy the solution of the above equation should make $\sin\theta_g = 0$. This occurs when

(i) $\theta_g = 2N_1\pi$ (N_1 is an integer) which is the resonance condition which leading to $T_{out} = T_{min}$.

(ii) $\theta_g = N_2\pi$ (N_2 is an odd integer) which leads to $T_{out} = T_{max}$.

At resonance $\theta_g = 2N_1\pi$, eqn. (33) reduces to

$$T_{min} = \frac{\alpha_{eff}^2 + g_{mo}^2\tau^2 - 2g_{mo}\alpha_{eff}\,\tau}{g_{mo}^2 + \alpha_{eff}^2\,\tau^2 - 2g_m\alpha_{eff}\,\tau} = \left(\frac{\alpha_{eff} - g_{mo}\,\tau}{g_{mo} - \alpha_{eff}\,\tau}\right)^2 \quad (34)$$

where g_{mo} is g_m evaluated at the resonance wavelength λ_o.

It is worth to mention here that according to eqn. (32c), the resonance condition $\theta_g = 2N_1\pi$ implies that the following two subconditions should satisfied simultaneously.

$$\tan\left(sL_{ps}\right) = 0 \quad (35a)$$

$$\beta_{ph}\, L - \delta\, L_{ps} = 2N_1\pi \quad (35b)$$

The first subcondition is satisfied when $sL_{ps} = N_3\pi$ where N_3 is a positive integer. Note that negative integer values for N_3 cannot be used since s and L_{ps} are positive. Recall that the coupling length $L_c = \pi/2s$. This implies that $L_{ps} = 2N_3L_c$ and hence L_{ps} is even number of the coupling length L_c. In this case, the optical power coupled from the silicon waveguide to the MDM plasmonic waveguide equals to zero at $z = L_{ps}$ (see eqn. (27)). This means that at the end of the phase shifter, the optical power is completely transfer from the hybrid waveguide to the silicon waveguide.

The second subcondition (eqn. 35b) can be used to estimate the resonance wavelength

$$\lambda_o = \frac{2\pi n_{ph} L}{N_1\pi + \delta L_{ps}} \quad (36a)$$

Thus the optical circumference of the ring $n_{ph}L$ is related to λ_o by

$$n_{ph}L = \left(N_1 + \delta L_{ps}/\pi\right)\frac{\lambda_o}{2} \quad (36b)$$

Investigating eqn. (36b) reveals the following facts

(i) N_1 should be a positive integer to yield a positive value for L.

(ii) For a given resonance wavelength, higher coupling efficiency between the two waveguides (i.e., δ is smaller) leads to a slightly shorter ring circumference.

(iii) The resonance condition in conventional optical resonators (i.e., the round trip optical length should be even number of resonance wavelength) is not satisfied in the resonator under investigation unless strong coupling between the two waveguide exists (i.e., $\delta = 0$).

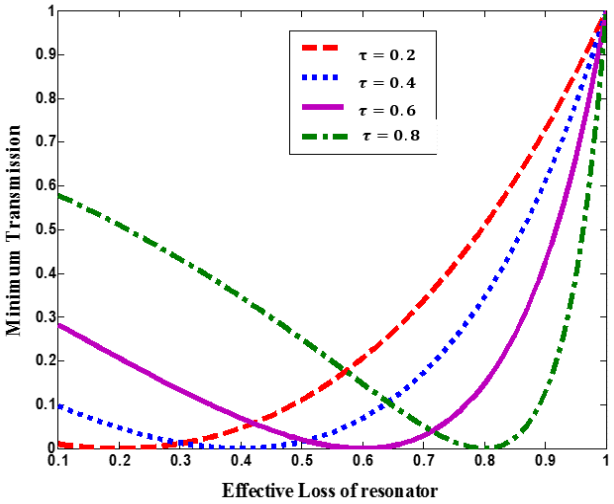

Figure 6. Relationship between minimum transmission and effective loss of theresonator

Using eqn. (35a) into eqn. (32b) yield $sg_{mo} \equiv g_m(\lambda_o) = 1$. Hence eqn. (34) is simplified to

$$T_{min} = \left(\frac{\alpha_{eff} - \tau}{1 - \alpha_{eff}\,\tau}\right)^2 \quad (37)$$

Note that T_{min} tends to zero at a critical coupling coefficient τ_c

$$\tau_c = \alpha_{eff} = \alpha e^{-L_{ps}/L_a} \quad (38)$$

Note further that T_{min} approaches 1 when $\alpha_{eff} = 1$ (i.e., lossless modulator) as shown in Fig. 6.

5. Bandwidth of the Transmission Characteristics

The analysis is carried further to determine the 3-dB bandwidth of the power transmission characteristics T_{out}. The maximum value of T_{out} occurs when $\theta_g = N_2\pi$ where N_2 is an odd integer

$$T_{max} = \left(\frac{\alpha_{eff} + \tau}{1 + \alpha_{eff}\,\tau}\right)^2 \quad (39)$$

The low and high half-power points θ_{g1} and θ_{g2} satisfy the relation

$T_{out}(\theta_{gi}) = 0.5T_{max}$, where i = 1 and 2.

After simplification, one gets

$$\cos\theta_{gi} = \frac{2(\alpha_{eff}^2 + g_m\tau^2)(1+\alpha_{eff}\,\tau^2)^2 - (g_m^2 + \alpha_{eff}^2\,\tau^2)(\alpha_{eff}+\tau)^2}{2g_m\alpha_{eff}\,\tau[2(1+\alpha_{eff}\,\tau)^2 - (\alpha_{eff}+\tau)^2]} \quad (40a)$$

Using the approximation $g_m = 1$ gives

$$\cos\theta_{gi} = \frac{2(\alpha_{eff}^2 + \tau^2)(1+\alpha_{eff}\,\tau^2)^2 - (1+\alpha_{eff}^2\,\tau^2)(\alpha_{eff}+\tau)^2}{2\alpha_{eff}\,\tau[2(1+\alpha_{eff}\,\tau)^2 - (\alpha_{eff}+\tau)^2]} \quad (40b)$$

Note that the solution of eqn. (40b), which is derived under the assumption of $g_m = 1$, yields $\theta_{g1} = -\theta_{g2}$. Therefore, the full width-at-half maximum (FWHM) bandwidth of the transmission spectrum $\Delta\lambda = 2|\theta_{g1}| = 2|\theta_{g2}|$.

The analysis of the transmission spectrum bandwidth $\Delta\lambda$ is extended further to obtain a simplified expression related to practical designs. For high efficiency operation, the design of the ring modulator should satisfy the following two requirements

(i) High-quality factor (Q) resonator to reduce the required applied voltage to switch the device from the ON state to OFF state (or vice versa).

(ii) Operation under critical coupling to ensure maximum extinction ratio.

The first requirement implies that θ_{gi} deviates slightly from the resonance condition $\theta_{go} = 2N_1\pi$ where N_1 is a positive integer. Therefore, θ_{gi} can be treated as a small angle relative to $\theta = 0^o$. Hence one can use the approximation $\cos\theta_{gi} \approx 1 - \frac{1}{2}\theta_{gi}^2$ to simplify eqn. (40b). The final result is

$$\theta_{gi} = \pm\left[\frac{2(C-D)}{C}\right]^{1/2} \quad (41a)$$

where

$$C = 2\alpha_{eff}\,\tau[2(1+\alpha_{eff}\,\tau)^2 - (\alpha_{eff}+\tau^2)^2] \quad (41b)$$

$$D = 2(\alpha_{eff}^2 + \tau^2)(1+\alpha_{eff}\,\tau)^2 - (1+\alpha_{eff}^2\tau^2)(\alpha_{eff}+\tau)^2 \quad (41c)$$

From eqn. (32c)

$$|\Delta\theta_g| \equiv |\theta_{g1} - \theta_{g2}| = L|\beta_{ph}(\lambda_1) - \beta_{ph}(\lambda_2)| \cong \frac{2\pi n_{ph} L}{\lambda_o^2}\Delta\lambda \quad (42)$$

where $\lambda_o = (\lambda_1\lambda_2)^{1/2}$ and can be considered as the resonance wavelength when $\lambda_1 \approx \lambda_2$. Here λ_1 and λ_2 denote the lower and upper half-power wavelengths, respectively.

Using eqn. (42) into eqn. (41) yields

$$\Delta\lambda = \frac{\lambda_o^2}{\pi n_{ph} L}\left[\frac{2(C-D)}{C}\right]^{1/2} \quad (43)$$

In deriving eqn. (43), the variation of the refractive index n_{ph} with wavelength is not taken into account and it is assumed that $\lambda_1 \approx \lambda_2$ for high Q-resonator. Otherwise, n_{ph} should be replaced by the group refractive index $n_{gph} = n_{ph} - \lambda\frac{\partial n_{ph}}{\partial\lambda}$.

It is worth to examine eqn. (43) under the condition of critical coupling where $\tau = \alpha_{eff}$. In this case

$$\Delta\lambda = \frac{\lambda_o^2}{\pi n_{ph} L}\frac{(1-\tau_c^2)}{\tau_c} \quad (44)$$

The resonance quality factor $Q_o \equiv (\lambda_o/\Delta\lambda)$ is given as

$$Q_o = \frac{\pi n_{ph} L}{\lambda_o}\left[\frac{C}{2(C-D)}\right] \quad (45a)$$

$$= \frac{\pi n_{ph} L \tau_c}{\lambda_o(1-\tau_c^2)} \quad \text{at critical coupling} \quad (45b)$$

Equations (43) and (45a) can be rewritten in another forms after using $\lambda_o = 2n_{ph} L/N_1$ (assuming strong coupling). The results are

$$\Delta\lambda = \frac{4n_{ph} L}{N_1^2\pi}\left[\frac{2(C-D)}{C}\right]^{1/2} \quad (46a)$$

$$Q_o = N_1\pi\left[\frac{C}{8(C-D)}\right]^{1/2} \quad (46b)$$

Under critical coupling

$$\Delta\lambda = \frac{4n_{ph} L}{N_1^2\pi}\frac{(1-\tau_c^2)}{\tau_c} \quad (46c)$$

$$Q_o = \frac{N_1\pi}{2}\frac{\tau_c}{(1-\tau_c)} \quad (46d)$$

Investigating eqns. (46) reveals that at fixed value of N_1, both λ_o and $\Delta\lambda$ are proportional to the resonator circumference. This leaves the quality factor to be independent of L. Note further that Q_o approaches ∞ when $\tau_c = 1$. This case corresponds to a lossless resonator where $\alpha_{eff} = 1$.

6. Chirp Characteristics

This section addresses the chirp (frequency modulation effect) when the device is used for analog intensity modulation. The phase characteristics of the output transfer function is governed by the following expression

$$\Theta_{out} = \tan^{-1}\left[\frac{g_m\,\tau\sin\Theta_g}{g_m\,\tau\cos\Theta_g - \alpha_{eff}}\right] - \tan^{-1}\left[\frac{g_m\sin\Theta_g}{g_m\cos - \alpha_{eff}\,\tau}\right] \quad (47)$$

The frequency chirp $(\Delta f)_{chirp}$ is related to Θ_{out} by

$$(\Delta f)_{chirp} = \frac{1}{2\pi}\frac{d\Theta_{out}}{dt} \quad (48a)$$

Since $\lambda f = c$ with c is the speed of light in vacuum, the wavelength chirp is then computed as

$$(\Delta\lambda)_{chirp} = -\frac{\lambda^2}{c}(\Delta f)_{chirp} \quad (48b)$$

Note that Θ_{out} is a function of the angle Θ_g which is a function of the applied voltage.

From eqn. (32c), it is clear that Θ_g is a function of $s = \pi/(2L_c)$ and the coupling length L_c is voltage dependent. Therefore, the frequency chirp can be calculated as

$$(\Delta f)_{chirp} = \frac{1}{2\pi}\left[\left(\frac{d\Theta_{out}}{d\Theta_g}\right)\left(\frac{d\Theta_g}{dL_c}\right)\left(\frac{dL_c}{dV_a}\right)\left(\frac{dV_a}{dt}\right)\right] \quad (49)$$

where V_a is the total applied voltage consisting of a bias voltage V_B and the ac modulating signal $V_m(t)$, $V_a(t) = V_B + V_m(t)$. Note that although the bias voltage does not affect dV_a/dt, it plays a key role in determining the chirp through the factor dL_c/dV_a.

From eqn. (47) and after using the relation $d\tan^{-1}x/dx = 1/(1+x^2)$, one gets

$$\frac{d\Theta_{out}}{d\Theta_g} = \frac{g_m\tau(D_1\cos\Theta_g - C_1\sin\Theta_g)}{C_1^2+D_1^2} + \frac{g_m(D_2\cos\Theta_g - C_2\sin\Theta_g)}{C_2^2+D_2^2} \quad (50)$$

where

$$C_1 = g_m\,\tau\sin\Theta_g \quad (51a)$$

$$D_1 = g_m\,\tau\cos\Theta_g - \alpha_{eff} \quad (51b)$$

$$C_2 = g_m\sin\Theta_g \quad (51c)$$

$$D_2 = g_m\cos\Theta_g - \alpha_{eff}\,\tau \quad (51d)$$

The factor $d\Theta_g/dL_c$ can be computed from

$$d\Theta_g/dL_c = \left(\frac{-2}{\pi}s^2\right)d\Theta_g/ds \quad (52a)$$

From eqn. (32c)

$$\frac{d\Theta_g}{ds} = \frac{L_{ps}(\delta/s)\sec^2(sL_{ps}) - (\delta/s^2)}{1+[(\delta/s)\tan(sL_{ps})]^2} \quad (52b)$$

Few remarks related to the chirp of the modulator under investigation are given here

(i) To reduce the chirp effect when the modulator is used for intensity modulation, the operating point (i.e., the bias voltage) should be chosen carefully to achieve low dL_c/dV_a value.
(ii) Positive DC voltage should be used to achieve low chirp intensity modulation.

7. Modulation Bandwidth

Three factors affect the modulation bandwidth of the modulator under investigation

(i) Modulator RC time constant
(ii) Modulator photon lifetime
(iii) Bandwidth limitation of the derive circuit.

Parallel-plate capacitance model can be used to estimate the modulator capacitance that seen between the two contacts

$$C_m = \frac{\varepsilon_o n_{poly}^2 L_{ps} H_{sl}}{W_{sl}} \quad (53)$$

where the relative permittivity (dielectric constant) of the polymer is taken as n_{poly}^2. Here ε_o represents the permittivity of the vacuum. Further H_{sl} and W_{sl} represent slot height and width, respectively. The bandwidth due to RC time constant is

$$B_{RC} = \frac{1}{2\pi RC_m}$$

where R is the loading resistance and sets to 50Ω in the simulation. Note that B_{RC} is directly proportional to slot width and inversely proportional to both slot height and phase shifter length.

The modulation bandwidth due to photon lifetime B_{plt} is related to photon life time τ_{ph} by [44]

$$B_{plt} = \frac{1}{2\pi\tau_{ph}} \quad (54)$$

The photon lifetime in optical resonator is related to its equality factor as follows. The quality factor is defined as [45]

$$Q_o = 2\pi \frac{\text{Stored energy}}{\text{Energy loss per cycle}} \quad (55)$$

The stored energy is lost at a rate of $1/\tau_{ph}$ (per unit time) which is equivalent to the rate $(1/\tau_{ph})T = 1/(\tau_{ph} f)$ per cycle, where T is the period of the optical wave. Therefore

$$Q_o = 2\pi f \tau_{ph} = 2\pi c\tau_{ph}/\lambda_o \quad (56a)$$

Thus

$$B_{plt} = \frac{c}{Q_o \lambda_o} \quad (56b)$$

Using eqn. (43) into eqn. (56b) yields

$$B_{plt} = \frac{c}{\pi n_{ph} L}\left[\frac{2(C-D)}{C}\right]^{1/2} \quad (57a)$$

Under critical coupling

$$B_{plt} = \frac{c}{\pi n_{ph} L}\frac{(1-\tau_c^2)}{\tau_c} \quad (57b)$$

Note that shorter L leads to higher B_{plt}.

8. Electrical Power Consumption

The electrical power dissipated during switching the modulator from one state (applied voltage = 0) to another state (applied voltage $= V_a$) can be considered mainly due to charging (or discharging) the modulator capacitor. To calculate this dissipated power, the modulator under investigation is modeled simply as a series RC network driven by a voltage source V_a through a switch S whose operating state (i.e., ON or OFF state) is controlled by the binary modulating bits (see Fig. 7).

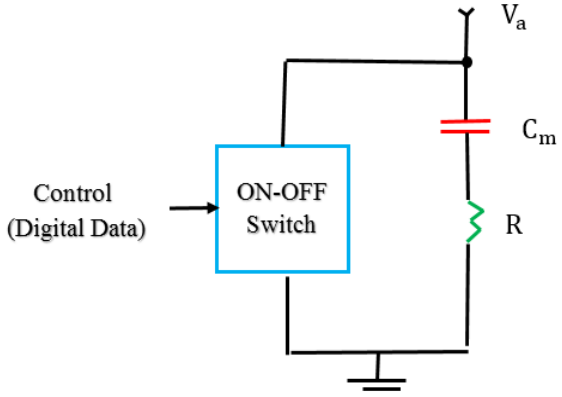

Figure 7. Simplified model to calculate the electrical power consumption during the switching modulator state

When the switch is turned off by the applied bit, the capacitor starts to charge gradually through the resistance R. During the transient time, the capacitance voltage $V_c(t)$ is given by

$$V_c(t) = V_a\left(1 - e^{-t/RC_m}\right) \quad (58a)$$

and the current passing through the RC circuit is

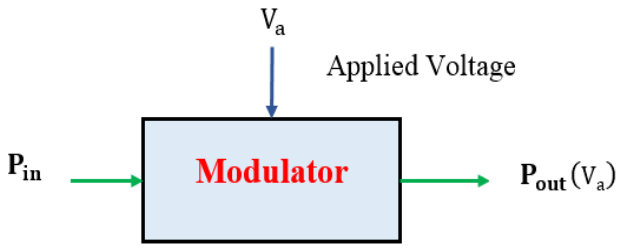

(a)

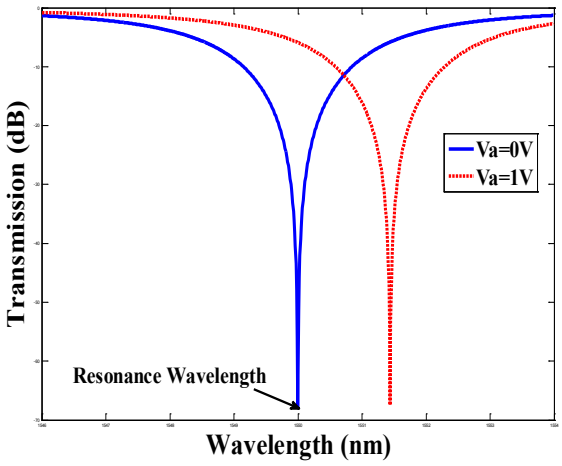

(b)

Figure 8. (a) Basic modulator model. (b) Modulator transmission characteristics versus wavelength

$$i(t) = C_m \frac{dV_c(t)}{dt} = \frac{V_a}{R} e^{-t/RC_m} \quad (58b)$$

The average power dissipated during one bit time $T_b = 1/B_r$, where B_r is the bit rate, can be calculated as

$$P_D = \frac{1}{T}\int_0^{T_b} Ri^2(t)\,dt = \frac{1}{2}C_m B_r V_a^2\left(1 - e^{-\frac{1}{RC_m B_r}}\right) \quad (59a)$$

For practical applications, the condition $T_b \gg RC_m$ and therefore

$$P_D \cong \frac{1}{2}C_m B_r V_a^2 \quad (59b)$$

Equation (59b) indicates clearly that the dissipated power scales linearly with the bit rate and with square of the applied voltage. Note that P_D is independent of the resistance R.

Few remarks related to the switching dissipated power P_D can be noted here

(i) The power consumption associated with discharging the modulator capacitance (i.e., the switch is off in Fig. 7) is also governed by eqn. (59).

(ii) In driving the modulator with real binary digital signal, the number of charge discharge cycles depends on the pattern of bits. In average, there is one complete charge/discharge cycle every four bits under the assumptions of equal numbers of "Ones" and "Zeros" are transmitted [46]. This can be understood by observing two successive bits which fall into four equally likely sequences (11, 00, 01 and 10). In the first two sequence, there is no change of state, so no energy is dissipated in charging the capacitance [46]. Therefore, the actual average dissipated power is $\overline{P}_D \cong \frac{1}{4}C_m B_r V_a^2$. In other words, the average dissipated energy per bit is given by

$$(\overline{E}_D)_{bit} = \frac{1}{4}C_m V_a^2 \quad (60)$$

(iii) To reduce the switching dissipated energy, one should design the modulator with small capacitance C_m. Note that the modulator capacitance depends only on the slot structure parameter (i.e., polymer refractive index n_{poly} and slot dimensions $L_{ps} H_{slot}/W_{slot}$).

(iv) If the stray capacitance due to the connection with driving circuit is included in the calculation, then the effective modulator capacitance increases and this will increase the dissipated power.

9. Extinction Ratio and Insertion Loss

Assume the modulator is excited by an optical signal having a wavelength equal to modulator resonance wavelength λ_o associated with zero applied voltage (i.e., $V_a = 0$). (See Fig. 8a). Figure 8b shows the transmission characteristics as a function of wavelength for two values of applied voltages. The applied voltage V_a shifts the resonance frequency. Positive values of V_a increases the polymer refractive index and hence introduce red shift to the resonance frequency.

In decibel scale, the insertion loss (IL) and extinction ratio (ER) are defined as

$$I_L = 10\log(P_{in}/P_{out}(V_a)) = -10\log|T(V_a)| \quad (61)$$

$$E_R = 10\log(P_{out}(V_a)/P_{out}(0)) \quad (62)$$

Note that

$$(P_{in}/P_{out}(V_a)) = (P_{in}/P_{out}(0)).(P_{out}(0)/P_{out}(V_a)).$$

Hence

$$I_L = I_{Lo} - E_R \text{ or } I_L + E_R = I_{Lo} \quad (63)$$

where I_{Lo} is the insertion loss when $V_a = 0$.

Note that the summation of insertion loss and extinction ratio is independent of applied voltage and it is equal to

$$I_{LO} = -10\log|T_{min}| \quad (64)$$

10. Conclusions

A design methodology has been explained for an optical ring modulator incorporating silicon-polymer-metal hybrid plasmonic phase shifter. Analytical expressions have been derived to characterize the transmission characteristics and performance parameters of this modulator. The results can be used as a guide line to design compact modulators for optical communication wavelengths.

ACKNOWLEDGMENTS

The work is a part of a PhD research program in the Institute of Laser for Postgraduate Studies, University of Baghdad, Iraq. One of the authors, Mrs. Al-mfrji, wishes to thank the College of Engineering at Al-Nahrain University, Baghdad, Iraq, for offering her the PhD scholarship.

REFERENCES

[1] Z. Zhou, X. Wang, H. Yi, Z. Tu, W. Tan, Q. Long, M. Yin and Y. Huang, "Silicon photonics for advanced optical communication systems," Optical Engineering, Vol. 52, No. 4, Article No. 045007, PP. 1-8, April 2013.

[2] H. Xu, X. Li, X. Xiao, Z. Li, Y. Yu, and J. Yu, "Demonstration and characterization of high-speed silicon depletion-mode Mach-Zehnder modulators," IEEE J. Selected Topics In Quantum Electronics, Vol. 20, No. 4, Article No. 3400110, PP. 1-10, August 2014.

[3] D. Petousi, L. Zimmermann, A. Gajda, M. Kroh, K. Voigt, G. Winzer, B. Tillack, and K. Petermann, "Analysis of optical and electrical tradeoffs of traveling-wave depletion-type Si Mach–Zehnder modulators for high-speed operation," IEEE J. Selected Topics In Quantum Electronics, Vol. 21, No. 4, Article No. 3400108, PP. 1-8, August 2015.

[4] H. Zhao, Y. Wang, A. Capretti, L. D. Negro, and J. Klamkin, "Broadband electroabsorption modulators design based on epsilon-near-zero indium tin oxide," IEEE J. Selected Topics In Quantum Electronics, Vol. 21, No. 4, PP. 3300207-33002014, August 2015.

[5] G. Gilardi, W. Yao, M. K. Smit, and M. J. Wale, "Observation of dynamic extinction ratio and bit error rate degradation due to thermal effects in integrated modulators," J. Lightwave Technology, Vol. 33, No. 11, PP. 2199-2205, June 2015.

[6] P. Wu, J. Novak, L. Jiang and Z. R. Huang, "Silicon electro-optic modulators using quantum tunneling structures," J. Lightwave Technology, Vol. 33, No. 1, PP. 25-33, January 2015.

[7] D. Sun, J. Zhang, C. Chen, M. Kong, J. Wang, and H. Jiang, "Theoretical feasibility demonstration for over 100GHz electro-optic modulators with c-axes grown $BaTio_3$ crystal thin-films," J. Lightwave Technology, Vol. 33, No. 10, PP. 1937-1947, January 2015.

[8] A. A. M. Saleh and J. M. Simmons, "Evolution toward the next-generation core optical network," J. Lightwave Technology, Vol. 24, No. 9, PP. 3303-3321, September 2006.

[9] J. Gosciniak and D. Tan, "Graphene-based waveguide integrated dielectric-loaded plasmonic electro-absorption modulators," Nanotechnology, Vol. 24, No. 18, PP. 185202-1852010, April 2013.

[10] S. Zhu, G. Q. Lo, and D. L. Kwong, "Theoretical investigation of silicon MOS-type plasmonic slot waveguide-based MZI modulators," Optics Express, Vol. 18, No. 26, PP. 27803-27819, December 2010.

[11] F. Li, M. Xu, X. Hu, J. Wu, T. Wang, and Y. Su, "Monolithic silicon-based 16-QAM modulator using two plasmonic phase shifters," Optics Communications, Vol. 286, PP. 166-170, January 2013.

[12] D. Korn, R. Palmer, H. Yu, P. C. Schindler, L. Alloatti, M. Baier, R. Schmogrow, W. Bogaerts, S. K. Selvaraja, G. Lepage, M. Pantouvaki, J. M.D. Wouters, P. Verheyen, J. V. Campenhout, B. Chen, R. Baets, P. Absil, R. Dinu, C. Koos, W. Freude, and J. Leuthold, "Silicon-organic hybrid (SOH) IQ modulator using the linear electro-optic effect for transmitting 16 QAM at 112 Gbit/s," Optics Express, Vol. 21, No. 11, PP. 13219-13227, June 2013.

[13] R. Palmer, L. Alloatti, D. Korn, P. C. Schindler, R. Schmogrow, W. Heni, S. Koenig, J. Bolten, T. Wahlbrink, M. Waldow, H. Yu, W. Bogaerts P. Verheyen, G. Lepage, M. Pantouvaki, J. Van Campenhout, P. Absil, R. Dinu, W. Freude, C. Koos, and J. Leuthold, "Silicon-organic hybrid MZI modulator generating OOK, BPSK and 8-ASK signals for up to 84 Gbit/s", IEEE Photonics, Vol. 5, No. 2, PP. 6600907-66009015, April 2013.

[14] D. Dai and S. He, "A silicon-based hybrid plasmonic waveguide with a metal cap for a nano-scale light confinement," Optics Express, Vol. 17, No. 19, PP. 16646-16653, September 2009.

[15] X. Sun, L. Zhou, H. Zhu, Q. Wu, X. Li, and J. Chen, "Design and analysis of a miniature intensity modulator based on a silicon-polymer-metal hybrid plasmonic waveguide," IEEE Photonics, Vol. 6, No. 3, Article No. 4801110, PP. 1-10, June 2014.

[16] S. Zhu, G. Q. Lo, and D. L. Kwong, "Theoretical investigation of ultracompact and athermal Si electro-optic modulator based on Cu-Tio_2-Si hybrid plasmonic donut resonator," Optics Express, Vol. 21, No. 10, PP. 12699-12712, May 2013.

[17] Y. Liu, J. Yan, and G. Han, "The transmission characteristic of metal–dielectric–metal slot waveguide-based nanodisk cavity with gain medium," IEEE Photonics, Vol. 7, No. 2, PP. 4500608-45006017, April 2015.

[18] V. J. Sorger, R. F. Oulton, R. Ma, and, X. Zhang, "Toward integrated plasmonic circuits," MRS Bulletin, Vol. 37, No. 1, PP. 728-737, August 2012.

[19] N. Kinsey, M. Ferrera, V. M. Shalaev, and A. Boltasseva, "Examining nanophotonics for integrated hybrid systems: a review of plasmonic interconnects and modulators using traditional and alternative materials," J. Optical Society of America B: Optical Physics, Vol. 32, No. 1, PP. 121-142, January 2015.

[20] H. M. G. Wassel, D. Dai, M. Tiwari, J. K. Valamehr, L. Theogarajan, J. Dionne, F. T. Chong, and T. Sherwood, "Opportunities and challenges of using plasmonic components in nanophotonic architectures," IEEE J. Emerging and Selected Topics in Circuits and Systems, Vol. 2, No. 2, PP. 154-168, June 2012.

[21] J. H. Choe and J. T. Kim, "Design of vanadium dioxide-based plasmonic modulator for both TE and TM modes," IEEE Photonics Technology Letters, Vol. 27, No. 5, PP. 514-517, March 2015.

[22] D. J. Thomson, F. Y. Gardes, J. M. Fedeli, S. Zlatanovic, Y. Hu, B. P. P. Kuo, E. Myslivets, N. Alic, S. Radic, G. Z. Mashanovich, and G. T. Reed, "50-Gb/s Silicon optical modulator," IEEE Photonics Technology Letters, Vol. 24, No. 4, PP. 234-236, February 2012.

[23] S. Pickus, S. Khan, C. Ye, Z. Li, and V Sorger, "Silicon plasmon modulators: breaking photonic limits,"IEEE Photonics Society Newsletter, PP. 4-10, December 2013.

[24] A. Melikyan, L. Alloatti, A. Muslija1, D. Hillerkuss, P. C. Schindler, J. Li, R. Palmer, D. Korn, S. Muehlbrandt, D. V. Thourhout, B. Chen, R. Dinu, M. Sommer, C. Koos, M. Kohl, W. Freude and J. Leuthold, "High-speed plasmonic phase modulators,"Nature Photonics, Vol. 8, No.9, PP. 229-233, March 2014.

[25] A. Melikyan, K. Koehnle, M. Lauermann, R. Palmer, S. Koeber, S. Muehlbrandt, P. C. Schindler, D. L. Elder, S. Wolf, W. Heni, C. Haffner, Y. Fedoryshyn, D. Hillerkuss, M. Sommer, L. R. Dalton, D. Van, W. Freude, M. Kohl, J. Leuthold, and C. Koos, "Plasmonic-organic hybrid (POH) modulators for OOK and BPSK signaling at 40 Gbit/s," Applied Optics, Vol. 23, No. 8, PP. 9938-9946 , April 2015.

[26] X. Sun, L. Zhou, X. Li, Z. Hong, and J. Chen, "Design and analysis of a phase modulator based on a metal–polymer–silicon hybrid plasmonic waveguide," Applied Optics, Vol. 50, No. 20, PP. 3428-3434 , July 2011.

[27] R. Thomas, Z. Ikonic, and R. W. Kelsall, "Electro-optic metal–insulator–semiconductor–insulator–metal Mach-Zehnder plasmonic modulator," Photonics and Nanostructures- Fundamentals and Applications, Vol. 10, No. 1, PP. 183-189, 2012.

[28] C. Haffner, W. Heni, Y. Fedoryshyn, D. L. Elder, A. Melikyan, B. Baeuerle, J. Niegemann, A. Emboras, A. Josten, F. Ducry, M. Kohl, L. R. Dalton, D. Hillerkuss, C. Hafner, and J. Leuthold, "High-speed plasmonic Mach-Zehnder modulator in a waveguide," ECOC 2014, Cannes – France PD.2.6.

[29] R. Thomas, Z. Ikonic, and R. W. Kelsall, "Plasmonic modulators for near-infrared photonics on a silicon-on-insulator platform," IEEE J. Selected Topics In Quantum Electronics, Vol. 19, No. 3, Article No. 4601708, PP. 1-8, June 2013.

[30] M. Morimoto, "Proposal for a plasmonic Mach–Zehnder modulatorutilizing quantum interference effect," IEEE J. Selected Topics In Quantum Electronics, Vol. 19, No. 6, PP. 33004071-33004072, December 2013.

[31] J. A. Dionne, K. Diest, L. A. Sweatlock, and H. A. Atwater, "PlasMOStor: a metal-oxide-Si field effect plasmonic modulator," Nano Letters, Vol. xx, No. x, PP. A-F, January 2009.

[32] C. Huang, R. J. Lamond, S. K. Pickus, Z. R. Li, V. J. Sorger, "A sub-λ-size modulator beyond the efficiency-loss limit," IEEE Photonics, Vol. 5, No. 4, PP. 22024111-220241112, August 2013.

[33] V. E. Babicheva, I. V. Kulkova1, R. Malureanu, K. Yvind, A. V. Lavrinenko, "Plasmonic modulator based on gain-assisted metal-semiconductor-metal waveguide, "Proc. SPIE 8627, Integrated Optics: Devices, Materials, and Technologies, Vol. XVII, No. 8627X, March 2013.

[34] X. Sun, L. Zhou, X. Li, J. Xie, and J. Chen, "Electrically tunable silicon plasmonic phase modulators with nano-scale optical confinement," Frontiers of Optoelectronics, Vol. 4, No. 4, PP. 359-363, 2011.

[35] F. Lou, D. Dai, L. Thylen, and L. Wosinski, "Design and analysis of ultra-compact EO polymer modulators based on hybrid plasmonic microring resonators," Applied Optics, Vol. 21, No. 17, PP. 20041-20051, August 2013.

[36] M. Xu, J. Wu, Z. Zhuang, F. Li, T. Wang, L. Zhou, and Y. Su, "Design of a silicon-plasmonic hybrid electro-optic modulator," Photonic Global Conference (PGC), No. 13308298, PP. 1-3, Singapore, December 2012.

[37] M. Xu, F. Li, T. Wang, J. Wu, L. Lu, L. Zhou, and Y. Su, "Design of an electro-optic modulator based on a silicon-plasmonic hybrid phase shifter," J. Lightwave Technology, Vol. 31, No. 8, PP. 1170-1177, April 2013.

[38] C. Li, C. Chen, M. Fiorentino, R. G. Beausoleil, B. Wang, and S. Palermo, "An energy efficient silicon microning resonator based photonic transmitter," IEEE Design and Test, Vol. 31, No. 5, PP. 46-54, May 2014.

[39] L. Zhang, Y. Li, J. Yang, M. Song, R. G. Beausoleil, and A. E. Willner, "Silicon-based microring resonator modulators for intensity modulation," IEEE J. Selected Topics In Quantum Electronics, Vol. 16, No. 1, PP. 149-158, February 2010.

[40] Y. Li, L. Zhang, M. Song, B. Zhang, J. Yang, R. G. Beausoleil, A. Willner, and P. Dapkus, "Coupled ring resonator based silicon modulator for enhanced performance,"Optics Express, Vol. 16, No. 17, PP. 13342-13348, August 2008.

[41] A. Yariv and P. Yeh, "Photonics: optical electronics in modern communications," Sixth Edition, Ch. 13, Oxford University Press, New York, 2007.

[42] W. Chang, "Fundamentals of guided-wave optoelectronics," Ch.2, Cambridge University Press, Cambridge 2010.

[43] M. L. Calvo and V. Lakshminarayanan, "Optical waveguides from theory to applied technologies, CRC press, London, 2007.

[44] J. Muller, F. Merget, S. S. Azadeh, J. Hauck, S. R. Garcia, B. Shen, and J. Witzens, "Optical peaking enhancement in high-speed ring modulators," Scientific Reports, PP. 1-9, September 2014.

[45] B. E. Saleh and M. C. Teich, "Fundamentals of optics," Second Edition, Ch. 10, John Wiley and Sons, New Jersey 2007.

[46] D. A. B. Miller, "Energy consumption in optical modulators for interconnects," Optics Express, Vol. 20, No. S2, PP. A293-A308, March 2012.